https://doi.org/10.5194/acp-2022-76
Preprint. Discussion started: 17 March 2022

Atmospheric Chemistry and Physics Discussions

Impact of Turbulence on Aeolian Sand and Dust Entrainment: Results from Wind-tunnel Experiment

Jie Zhang[1,*], Guang Li[1,2,3,*], Li Shi[1], Ning Huang[1], and Yaping Shao[4]

[1]Key Laboratory of Mechanics on Disaster and Environment in Western China, Lanzhou University, Lanzhou 730000, China
[2]College of Atmospheric Science, Lanzhou University, Lanzhou 730000, China
[3]College of Architecture Civil and Environmental Engineering, Ecole Polytechnique Federal de Lausanne, Lausanne 1015, Switzerland
[4]Institute for Geophysics and Meteorology, University of Cologne, Germany
[*]These authors contributed equally to this work.

Correspondence: Yaping Shao (yshao@uni-koeln.de)

Abstract. We hypothesize that large eddies play a major role in the entrainment of aeolian sand and dust particles. To test this, wind-tunnel experiments are carried out to measure the entrainment rate of various particle sizes under different flow conditions. Wind tunnel flows are usually neutrally stratified with no large eddies which typically develop in convective atmospheric boundary layers. Here, a novel technique is applied by deploying a piece of randomly fluttering cloth to generate large eddies similar to convective eddies in atmospheric boundary layers, which we call quasi-convective turbulence. The characteristics of quasi-convective turbulence are analyzed with respect to neutral turbulence in the Monin-Obukhov similarity framework, and the probability distributions of surface shear stress are examined. We show that for given mean flow speed and in comparison with neutral flow conditions, quasi-convective turbulence increases the surface shear stress and alters its probability distribution, and hence substantially enhances the entrainment of sand and dust particles. Our hypothesis is thus confirmed by the wind-tunnel experiments. We also explain why large eddies are important to aeolian entrainment and transport.

1 Introduction

The entrainment of sand and dust particles is among the most important quantities to determine in aeolian studies. Based on Bagnold (1941), Owen (1964) showed that the vertically integrated saltation flux, Q, can be expressed as

$$Q = \begin{cases} c_0 \frac{\rho}{g} u_*^3 (1 - \frac{u_{*\mathrm{t}}^2}{u_*^2}) & \text{for } u_* > u_{*\mathrm{t}} \\ 0 & \text{otherwise} \end{cases} \quad (1)$$

where c_0 is the Owen coefficient, ρ air density, g acceleration due to gravity, u_* friction velocity and $u_{*\mathrm{t}}$ threshold friction velocity. By definition, $u_* = \sqrt{\tau/\rho}$ is a descriptor of the surface shear stress, τ. It has been shown in numerous studies that

https://doi.org/10.5194/acp-2022-76
Preprint. Discussion started: 17 March 2022


Atmospheric Chemistry and Physics Discussions

Eq. (1) is valid in general, but c_0 scatters over a wide range if Eq. (1) is fitted to Q observations (Gillette et al., 1996, 1997; Leys, 1998; Liu et al., 2018). While the large scatter of c_0 is not yet fully explained, it is most likely because both u_* and $u_{*\mathrm{t}}$ are stochastic variables and hence saltation driven by atmospheric boundary-layer (ABL) turbulent flows is also turbulent (Butterfield, 1991, 1998). In this sense, Eq. (1) is valid only for mean quantities, $\overline{Q}$ and $\overline{u}_*$, if we assume $u_{*\mathrm{t}}$ is constant [this assumption is sufficient for the purpose of our study, but see Shao (2008), Raffaele et al. (2016), Liu et al. (2018), and Li et al. (2020) for discussions on $u_{*\mathrm{t}}$ as a stochastic variable].

Our question here is how turbulence influences the entrainment of sand and dust particles into the atmosphere. Numerous studies on aerodynamic sand and dust entrainment have been carried out (e.g., Greeley and Iversen, 1987; Anderson and Haff, 1988, 1991; Loosmore and Hunt, 2000; Doorschot and Lehning, 2002; Jia and Wang, 2021), but in all these studies, flow is assumed to be steady and the impact of turbulence on the entrainment is neglected. In reality, atmospheric flows are always turbulent, and aeolian processes also. Butterfield (1991, 1998) investigated the behavior of saltating grains in unsteady flows and found that both the frequency and strength of wind gusts influence the rate of sand transport. Stout and Zobeck (1997) observed that saltation intermittently occurs even when $u_* < u_{*\mathrm{t}}$, a phenomenon known as saltation intermittency. Xuan (2004) concludes that turbulence decreases $u_{*\mathrm{t}}$ or the threshold wind velocity u_t and increases Q or the vertical flux (the dust emission rate). Klose and Shao (2012) and Klose et al. (2014) developed a parameterization scheme for dust emission by convective turbulence and explained how dust emission can be produced by large eddies in weak mean wind conditions. Comola et al. (2019) draw on extensive field measurements to show that neglecting saltation intermittency causes biases in the timing and intensity of predicted fluxes. Shao et al. (2020) reported that saltation in unstable ABLs is generally more fully developed than in stable ABLs.

It should be pointed out that saltation intermittency in the sense of Stout and Zobeck (1997) is a special case of saltation fluctuation at $u_* \sim u_{*\mathrm{t}}$, because in general if $u_* = \overline{u}_* + u_*^{'}$ and suppose $u_*^{'} > 0$, then $Q = Q(\overline{u}_*) + Q^{'}$ with $Q^{'} > 0$. The saltation intermittency Stout and Zobeck (1997) studied is for the case $\overline{u}_* = u_{*\mathrm{t}}$ and $Q(\overline{u}_*) = 0$ but $Q^{'} > 0$. The above discussion suggests that the turbulent (or probabilistic) behavior of u_* is of great importance to Q and naturally also to sand and dust entrainment. Because the turbulent behavior of u_* is closely related to ABL turbulence, our hypothesis is thus that ABL turbulence profoundly influences the entrainment of sand and dust particles.

In stable and neutral ABLs, turbulence is generally weak and more homogeneous and isotropic, but in unstable (or convective) ABLs, strong due to buoyancy production of turbulent kinetic energy and less homogeneous and isotropic due to the presence of large eddies. It is therefore particularly interesting to study the influences of convective turbulence on aeolian processes. Khalfallah et al. (2020) pointed out that dust particle size at emission is dependent on ABL stability. Shao et al. (2020) compared some features of saltation and dust emission in convective and stable ABLs based on the field observations of the Japan-Australian Dust Experiment (JADE, Ishizuka et al., 2008, 2014), but due to the limitations of the field measurements, the role of turbulence in aerodynamic sand and dust entrainment could not be explicitly examined. We are thus motivated to acquire additional data to test our hypothesis.

Wind tunnel is a powerful tool for studying aeolian problems under controlled flow conditions (Rasmussen and Mikkelsen, 1991; Alfaro et al., 1997; Brown et al., 2008; Zhang et al., 2014). However, wind-tunnel experiments are often limited to neutral

https://doi.org/10.5194/acp-2022-76
Preprint. Discussion started: 17 March 2022

Atmospheric Chemistry and Physics Discussions

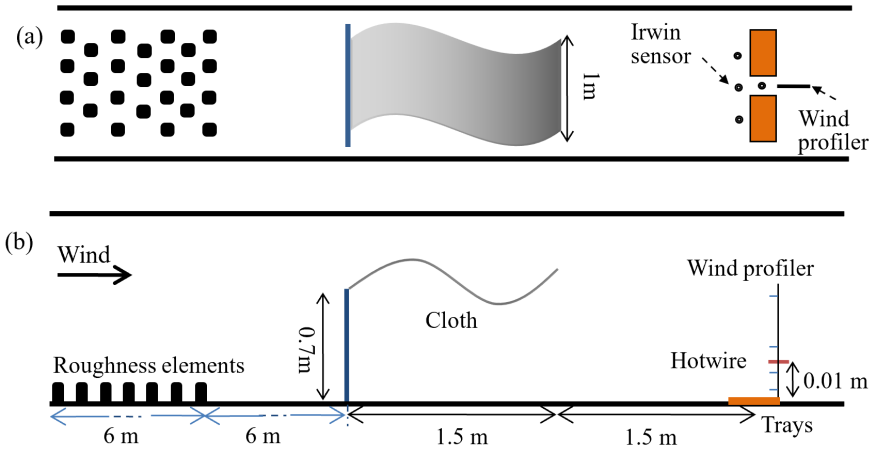

Figure 1. (a) Top view of the wind-tunnel configuration; (b) Side view of the wind-tunnel configuration. A piece of randomly fluttering cloth in the wind tunnel enables the generation of quasi-convective turbulence.

flows because most wind tunnels do not have the capacity of generating convective eddies. Here we apply a simple forced-perturbation technique (using a piece of randomly fluttering cloth) to generate quasi-convective turbulence, namely, turbulence in a neutrally stratified flow but with characteristics of convective turbulence. Aerodynamic sand and dust entrainment rates under various mean-wind and quasi-convective turbulence conditions are measured. We use these wind-tunnel data to study how and why turbulence influences the aerodynamic sand and dust entrainment rate.

2 Wind-tunnel Experiment and Instrumentation

We carried out the experiment in the Lanzhou University wind tunnel which is specially designed for aeolian studies. The technical details of the wind tunnel can be found in Zhang et al. (2014) and hence only the most relevant information is given here. Fig.1 shows the wind-tunnel configuration for the experiment. The working section of the tunnel is about 15 m long, with the first 6 m being the roughness-element section for generation of a turbulent boundary layer. One end of the piece of cloth is attached to a horizontal bar located 6 m downstream the roughness-element section and 0.7 m above the tunnel floor, and the other end is allowed to flutter freely. Two trays (285 mm wide, 150 mm long and 13 mm deep) are placed 1.5 m downstream the end of the fluttering cloth. The trays filled with sand are mounted flush to the tunnel floor. Each tray is placed on an electronic balancer which measures the mass loss from the tray with a precision of 0.01 g in the range 5 kg. Four Irwin sensors are mounted in front and between the trays and a wind profiler is located between the trays, next to a hotwire anemometer fixed at 10 mm height.

The wind profiler is a rack of ten pitot tubes placed at the levels of 6.5, 10, 15, 30, 60, 120, 201, 351 and 501 mm above the tunnel floor for measuring the profile of the mean flow speed, while the hotwire anemometer measures turbulent fluctuations

https://doi.org/10.5194/acp-2022-76
Preprint. Discussion started: 17 March 2022


Atmospheric Chemistry and Physics Discussions

with a sampling frequency of 1000 Hz. Irwin sensors (Irwin, 1981) are omnidirectional devices for measuring the surface shear stress, which have been used successfully in a number of earlier studies (e.g. Wu and Stathopoulos, 1993; Walter et al., 2012). We manufactured the Irwin sensors used in this study ourselves according to the dimensions given in Gillies et al. (2007). The Irwin-sensor pressure differences are sampled at a frequency of 100 Hz using a scan valve attached to a pressure transducer (ZOC33). Prior to the wind-tunnel experiment, the Irwin sensors are calibrated in the wind-tunnel against the wind profiler for various flow conditions, by comparison of the shear stresses measured by the two devices.

A key requirement for our experiment is to generate turbulence in the wind tunnel with characteristics similar to convective turbulence. In convective ABLs, large eddies develop due to buoyancy production of turbulent kinetic energy. While horizontal velocity fluctuations are approximately Gaussian distributed, vertical velocity fluctuations are typically non-Gaussian with a positive skewness. Convective turbulence is difficult to generate in wind-tunnel flows which are usually neutrally stratified. In our experiment, we use a 'forced perturbation' technique to generate turbulence in the wind-tunnel flow, that has the characteristics similar to convective turbulence, in particular, with energy containing large eddies and a positively skewed asymmetric probability distribution function (PDF). Such turbulence is here referred to as quasi-convective turbulence. Forced perturbation is achieved by using a piece of cloth which flutters randomly in the wind-tunnel flow to produce small eddies, and flaps irregularly to produce large eddies, superposed on the background turbulence. Although quasi-convective turbulence is not the same as convective turbulence, the forced-perturbation method is both simple and efficient to remedy the critical deficit of wind-tunnel flows which lack of large eddies.

The wind tunnel is a blow tunnel, with the inlet flow speed controlled by a rotating fan. For our experiment, the fan speed is fixed for each run between 7000 and 12000 rpm. We call the runs with forced perturbation WP-runs and those with no forced perturbation NP-runs. The entrainment of four particle size groups are measured for various flow and turbulence combinations, as listed in Table 1. For each run, at least three successful repetitions are made and the measurement period for each repetition is 5 minutes. Four different soils are used in the experiment, labelled as S1, S2 etc. The mean particle size of the four soils are 75, 140, 215 and 398 μm. The particle size distributions are approximately log-normal. We use NP07_S1 to denote the NP-run for fan speed 7000 rpm and soil S1 and name following this convention the other runs.

2.1 Results

2.1.1 Forced Perturbation

We first examine whether turbulence generated using the forced-perturbation technique has the desired features of convective turbulence. In Fig. 2, the characteristics of $V_{10\mathrm{mm}}$ (flow velocity sensed by the hotwire anemometer) are compared between the NP07_O and WP07_O runs, including its time series, PDF and power spectrum. As $V_{10\mathrm{mm}}$ is measured using a one-dimensional hotwire, it is the resultant velocity of its horizontal component, $u_{10\mathrm{mm}}$, and vertical component, $w_{10\mathrm{mm}}$. As seen, the force-perturbation technique effectively generates quasi-convective turbulence, as turbulence for the WP07_O run has an increased variance and a positive skewness, while turbulence for the NP07_O run is weaker and almost Gaussian distributed.

https://doi.org/10.5194/acp-2022-76
Preprint. Discussion started: 17 March 2022

Atmospheric Chemistry and Physics Discussions

Table 1. Summary of wind-tunnel experiments

Particle size \ Fan speed (×1000 rpm)	Repetitions									
	7 NP/WP	7.5 NP/WP	8 NP/WP	8.5 NP/WP	9 NP/WP	9.5 NP/WP	10 NP/WP	10.5 NP/WP	11 NP/WP	12 NP/WP
O (no soil)	1	/	1	/	1	/	1	/	1	1
S1 (75 μm)	5/3	/	5/5	/	5/5	/	5/5	/	5/5	3/5
S2 (140 μm)	5/5	/5	5/5	/4	5/5	3/3	3/	/	/	/
S3 (215 μm)	5/5	/	5/5	/5	5/5	/	5/5	5/	6/	/
S4 (398 μm)	3/3	/	3/5	/	3/5	/	5/5	/	5/5	5/

NP = no perturbation; WP = with perturbation.

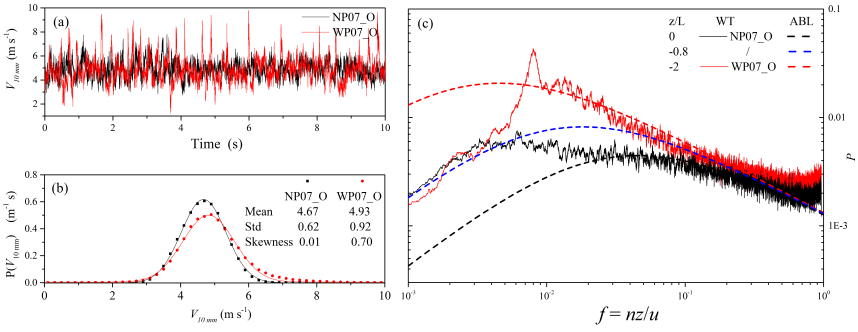

Figure 2. (a) A section of 10s of the $V_{10\mathrm{mm}}$ time series for the NP07_O and WP07_O runs; (b) probability density functions of $V_{10\mathrm{mm}}$ (estimated using a time series of 300s); (c) normalized power spectra of $V_{10\mathrm{mm}}$ for WP07_O and NP07_O compared with field-observed power spectra in atmospheric boundary layer (Kaimal et al., 1972). $Z_{0\mathrm{WT}}$ is 1.33×10^{-2} mm and $Z_{0\mathrm{ABL}}$ is set to 3.10 mm (Wiernga, 1993).

In the MOST (Monin-Obukhov Similarity Theory) framework, $\zeta = z/L$, with z being height and L the Obukhov length, is used as a measure of ABL stability: the ABL is stable, neutral and unstable for $\zeta > 0$, $= 0$ and < 0, respectively. Kaimal et al. (1972) examined the characteristics of surface-layer turbulence using the MOST and found that the nondimensionalized power spectra of ABL quantities collapse to universal functions with ζ being the only parameter. They showed that as the ABL stability decreases, the inertial subrange extends to lower frequencies. Plotted in Fig. 2(c) are the normalized power spectra of V_{10mm} for WP07 and NP07, denoted as PWP07 and PNP07, respectively. Following Kaimal et al. (1972), we express the normalized frequency as $f = nz/u$ (with n being frequency) and normalized energy spectral density as

$$P = nS(n)\overline{u}_*^{-2}\phi_\epsilon^{-2/3} \quad (2)$$

https://doi.org/10.5194/acp-2022-76
Preprint. Discussion started: 17 March 2022


Atmospheric Chemistry and Physics Discussions

with S being the energy density per frequency and ϕ_ϵ the MOST similarity function for the dissipation rate of turbulent kinetic energy

$$\phi_\epsilon = 1 + 0.5\,|\zeta|^{2/3} \tag{3}$$

following Kaimal and Finnigan (1994), our analysis does not involve the cases of $\zeta > 0$. For the wind-tunnel runs, $nS(n)$ is obtained by analyzing the horizontal wind velocity component measured by the hotwire, $\overline{u}_*$ is measured by the Irwin sensor and ϕ_ϵ is calculated by using Eq. (3) with ζ = 0 for the NP07_O run and ζ = -2 for the WP07_O run. For comparison, the ABL velocity power spectra, denoted as PABL, for three different stabilities ζ = 0, -0.8 and -2 are plotted. An empirical form given by Kaimal et al. (1972)

$$P_{\mathrm{ABL}} = 105 f/(a + 33 f)^{5/3} \tag{4}$$

where a is an empirical constant set to 1, 0.4 and 0.1 for ζ = 0, -0.8 and -2, respectively. Note that in Fig. 2(c), $P_{\mathrm{ABL}} \times z_{0\mathrm{WT}}/z_{0\mathrm{ABL}}$ is plotted, where $z_{0\mathrm{WT}}$ is the roughness length for the wind-tunnel flows and $z_{0\mathrm{ABL}}$ that for the ABL flows. The ratio z_0/L is the MO number which was excluded in Kaimal et al. (1972) and the exclusion is justified because the differences in z_0 in their data are not large. However, because $z_{0\mathrm{WT}}$ (Table 2) is two orders of magnitude smaller than $z_{0\mathrm{ABL}}$, the effect of z0/L needs to be considered and hence the mentioned multiplication is necessary.

Fig. 2(c) reveals that P_{NP07} and P_{WP07} are almost the same in the (normalized) frequency range of $f < 3 \times 10^{-3}$, as turbulence in this frequency range is attributed to the upstream roughness elements. They are also the almost the same in the high frequency range of $f > 0.1$. In the energy containing range $3 \times 10^{-3} < f < 0.1$, P_{WP07} shows much increased energy with respect to P_{NP07}, implying that the forced perturbation technique generated large eddies in the wind-tunnel flow.

Fig. 2(c) also shows that it is generally difficult for the wind tunnel to reproduce the turbulence observed in the ABL. Clearly, compared with $P_{\mathrm{ABL}}(\zeta$ = -0.8) and $P_{\mathrm{ABL}}(\zeta$ = -2), P_{NP07} lacks energy in the frequency range of 3×10^{-3} 1×10^{-1}. In contrast, power spectral density in this frequency range is substantially increased if forced perturbation is applied as a comparison of P_{WP07} and P_{NP07} reveals. It is seen that P_{WP07} is fairly similar to $P_{\mathrm{ABL}}(\zeta$ = -2), although it still lacks energy for $f < 10^{-2}$. In summary, Fig. 2 shows that the forced-perturbation technique is effective in generating quasi-convective turbulence which has a degree of similarity with ABL convective turbulence. This simple technique can be further optimized (e.g. by using a combination of fluttering cloths of different materials and different dimensions) to overcome the critical lack of convective eddies in wind-tunnel flows, which has so far seriously limited the usefulness and generalization of the wind-tunnel results.

2.1.2 Mean Wind Profile and Shear Stress

Fig. 3 shows the mean wind profiles measured using the pitot tubes. For height z smaller than 0.2 m, the mean wind profiles are for both NP runs and WP runs are approximately logarithmic. In the WP runs, the flow speed for z > 0.2 m is reduced due to the fluttering cloth which acts as a momentum sink. For a given fan speed, the fluttering cloth not only enhances the turbulent kinetic energy (Fig. 2) but also modifies the wind profile for z < 0.2 m to one more similar to wind profile in convective ABL.

https://doi.org/10.5194/acp-2022-76
Preprint. Discussion started: 17 March 2022

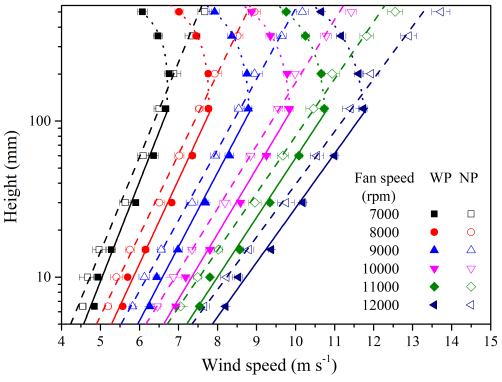

Figure 3. Mean flow speed profiles for different fan speeds and the NP and WP runs

Based on the MOST, the similarity relationship between the mean flow speed, $\overline{U}$, can be expressed as

$$\overline{U}(z) = \overline{u}_*/\kappa[ln(z/z_0) + \Psi_{\rm m}] \tag{5}$$

where κ is the von Karmen constant, and

$$\Psi_{\rm m} = \int_{z_0}^{z} (1-\phi_{\rm m}) dlnz \tag{6}$$

and

$$\phi_{\rm m} = (1-\gamma_{\rm m}\zeta)^{-1/4}, \zeta \leq 0 \tag{7}$$

being the similarity function. For ABL flows, $\gamma_{\rm m}$ = 16 is an empirical coefficient (Businger et al., 1971). For the NP runs, $\Psi_{\rm m}$ = 0 is assumed. By fitting Eq. (5) to $\overline{U}$ measured at z < 0.2 m, we estimate $\overline{u}_*$ and z_0. The shear stress $\overline{\tau} = \rho\overline{u}_*^2$ (here, air density $\rho = 1.2{\rm kgm}^{-3}$) is then used to calibrate the shear stress measured using the Irwin sensor, $\overline{\tau}_{\rm Irwin}$. For the WP runs, $\Psi_{\rm m}$ cannot be set to zero due to the quasi-convective turbulence generated, but as both $\gamma_{\rm m}$ and L are unknown for the quasi-convective turbulent flows, it is sensible to write Eq. (7) as

$$\phi_{\rm m} = (1-\eta_{\rm m} z)^{-1/4} \tag{8}$$

with $\eta_{\rm m} \sim \gamma_{\rm m}/L$. By combining the $\overline{U}$ measurements at z < 0.2 m and the shear stress measured using the Irwin sensors for the WP runs, $\eta_{\rm m}$ can be estimated. The results are summarized in Table 2.

Table 2 shows that forced perturbation leads to a slightly increased $\overline{u}_*$. The deployment of the forced-perturbation technique results in an increase of $\overline{\tau}$ by about 25% at fan speed 7000 rpm to about 15% at fan speed 12000 rpm. As pointed out in several earlier studies Klose and Shao (2012), Li et al. (2020) and Shao et al. (2020), we emphasis again that surface shear stress τ is

https://doi.org/10.5194/acp-2022-76
Preprint. Discussion started: 17 March 2022

Atmospheric Chemistry and Physics Discussions

Table 2. Friction velocity $\overline{u}_*$ and roughness length z_0 estimated for runs with and with no forced perturbation and different wind-tunnel fan speeds.

Fan speed	NP		WP			
	Profile($\Psi_m = 0$)		Profile($\Psi_m \neq 0$)		Irwin	
(×1000 rpm)	u_* (ms^{-1})	z_0 (mm)	u_* (ms^{-1})	z_0 (mm)	η_m (mm^{-1})	u_* (ms^{-1})
7	0.29	0.0133	0.31	0.0147	-0.0229	0.32
7.5	/	/	0.34	0.0151	-0.0213	0.34
8	0.34	0.0146	0.36	0.0158	-0.0200	0.37
8.5	/	/	0.39	0.0166	-0.0188	0.39
9	0.38	0.0159	0.41	0.0156	-0.0178	0.42
9.5	0.40	0.0125	0.44	0.0165	-0.0168	0.44
10	0.43	0.0164	0.46	0.0166	-0.0160	0.47
10.5	0.47	0.0207	/	/	/	/
11	0.47	0.0176	0.50	0.0165	-0.0145	0.51
12	0.51	0.0166	0.55	0.0162	-0.0133	0.55

a stochastic variable, which satisfies a probability distribution function $p(\tau)$. To facilitate discussions, we explicitly write

$$\tau = \overline{\tau} + \tau' \tag{9}$$

with τ' being the perturbation of τ.

2.1.3 Aeolian Sand/Dust Entrainment in Quasi-convective Turbulence

The emission rate of sand and dust particles, F, is estimated from the mass loss of the trays as

$$F = \frac{1}{I}\sum_{i=1}^{i=I}\frac{\Delta m_i}{A\Delta T_i} \tag{10}$$

where Δm_i is the mass loss from the tray during in the ith run with runtime ΔT_i, A is the tray surface area and I is the number of repetitions. Fig. 4 shows that the emission rates of the various particle-size groups measured in the NP and WP runs. It is seen that for all four soils, for given $\overline{\tau}$, the emission rate for the WP runs are substantially larger than that for the NP runs. This result suggests that in addition to the mean surface shear stress, $\overline{\tau}$, the surface shear stress perturbations, τ', significantly influence the emission rate, F. As τ' is related to the structure of boundary-layer turbulence, it can be stated that the structure of boundary-layer turbulence significantly influences the entrainment rate: for a given mean surface shear stress, convective turbulence is much more efficient in lifting particles from the surface into the air. This finding is consistent

https://doi.org/10.5194/acp-2022-76
Preprint. Discussion started: 17 March 2022

Atmospheric Chemistry and Physics Discussions

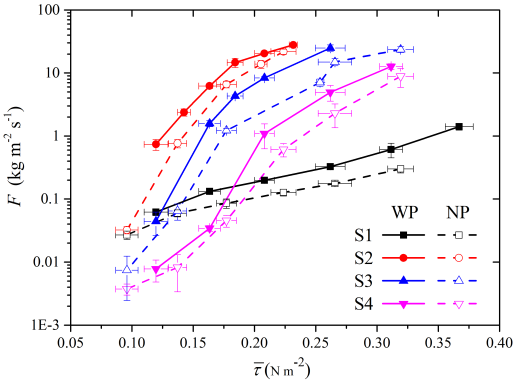

Figure 4. Emission rate of four different soils observed in the NP and WP runs. Hollow symbols represent the WP runs and solid symbols for the NP runs.

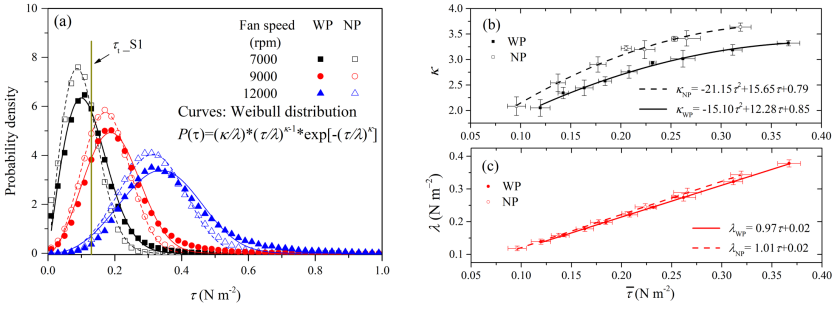

Figure 5. (a) Probability density function of surface shear stress τ for NP and WP runs with fan speed 7000, 9000 and 12000 rpm. The dashed gray line marks the threshold shear stress for S1 (τ_t_S1). The symbols are the results from the Irwin sensors and curves the Weibull distributions. By fitting the Weibull distributions to the respective data of the various runs, the corresponding shape and scaling parameters are estimated and plotted against the mean shear stress $\overline{\tau}$ in (b) and (c), respectively.

with the observations of the Japan-Australian Dust Experiment (JADE), as presented in the recent study of Shao et al. (2020), i.e., aeolian sand transport and dust emission are much more intensive in convective ABLs than in stable ABLs. Using the τ measurements of the Irwin sensor, we estimate the PDF of τ, $p(\tau)$. Klose et al. (2014) and Shao et al. (2020) suggested that $p(\tau)$ is approximately Weibull distributed and positively skewed. Fig. 5 show as example $p(\tau)$ for the NP and WP runs for fan speed 7000, 9000 and 12000 rpm. As seen, the forced-perturbation results in significantly different PDF of τ by slightly increasing $\overline{\tau}$ and clearly increasing the probability of large τ. It is this increase in the probability of large τ, that explains the differences between the $F \sim \overline{\tau}$ dependency between the NP and WP runs seen in Fig. 4. The structure of ABL turbulence, reflected here in $p(\tau)$, significantly influences the sand and dust entrainment and saltation fluxes, because these aeolian quantities depend

https://doi.org/10.5194/acp-2022-76
Preprint. Discussion started: 17 March 2022

Atmospheric Chemistry and Physics Discussions

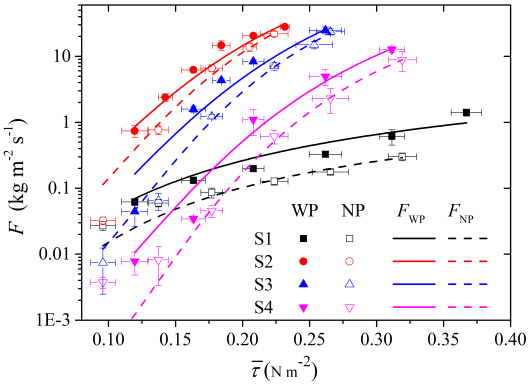

Figure 6. Estimated entrainment rates with and without forced perturbation. The dots are experimental data and lines derive from Eq. (12).

non-linearly on τ. As explained in (Shao, 2008, sect 6.12.4), for a given particle size, the entrainment rate F can be expressed as

$$F = \gamma\sqrt{\tau/\rho}(\tau - \tau_t) \tag{11}$$

with γ being an empirical efficiency parameter for dust entrainment, and τ_t is the threshold shear stress for particle entrainment. The threshold is in general a stochastic variable (Raffaele et al., 2016; Liu et al., 2018), but for simplicity, we assume it is constant for given particle size. To account for the fluctuations of τ, we estimate

$$F = \int_{\tau_t}^{\infty} \gamma\sqrt{\tau/\rho}(\tau - \tau_t)p(\tau)d\tau \tag{12}$$

for the four soils S1, S2, S3 and S4 tested, τ_t is estimated to be 0.13 $\mathrm{Nm^{-2}}$, 0.27 $\mathrm{Nm^{-2}}$, 0.31 $\mathrm{Nm^{-2}}$ and 0.35 $\mathrm{Nm^{-2}}$, respectively. Fig. 6 shows that Eq. (12) fits well to the measurements for all runs. Eq. (12) reveals that convective turbulence may influence both the efficiency parameter γ, and the statistical behavior of the term, $\int_{\tau_t}^{\infty} \gamma\sqrt{\tau/\rho}(\tau - \tau_t)p(\tau)d\tau$. To facilitate discussion, we write Eq. (12) as

$$F = \overline{\gamma} \int_{\tau_t}^{\infty} \sqrt{\tau/\rho}(\tau - \tau_t)p(\tau)d\tau \tag{13}$$

A comparison of $\overline{\gamma}$ for NP and WP runs are shown in Table 3. It is seen, that $\overline{\gamma}$ is significantly increased for the WP runs, in particular for soils S1 and S4. Next, we estimate the ratio σ_F defined as

$$\sigma_F = \int_{\tau_t}^{\infty} \sqrt{\tau/\rho}(\tau - \tau_t)p_{WP}(\tau)d\tau \Big/ \int_{\tau_t}^{\infty} \sqrt{\tau/\rho}(\tau - \tau_t)p_{NP}(\tau)d\tau \tag{14}$$

Fig.7 shows the relationship between σ_F and excess surface shear stress $(\overline{\tau} - \tau_t)$. A negative exponential law appears to exist. For the conditions with $\overline{\tau} > \tau_t$ (corresponding to the continuous entrainment defined by Li et al. 2020), σ_F is close to one,

https://doi.org/10.5194/acp-2022-76
Preprint. Discussion started: 17 March 2022

Atmospheric Chemistry and Physics Discussions

Table 3. Threshold shear stress τ_t and empirical parameter γ for test surfaces.

soil type	$\tau_t(\mathrm{Nm}^{-2})$	$\overline{\gamma_{NP}}(\mathrm{m}^{-2}\mathrm{s}^2)$	$\overline{\gamma_{WP}}(\mathrm{m}^{-2}\mathrm{s}^2)$	$\overline{\gamma_{NP}}/\overline{\gamma_{WP}}$
S1	0.13	3.00	8.25	2.75
S2	0.27	3560.86	4121.62	1.16
S3	0.31	2818.35	3584.11	1.23
S4	0.35	695.08	1282.87	1.85

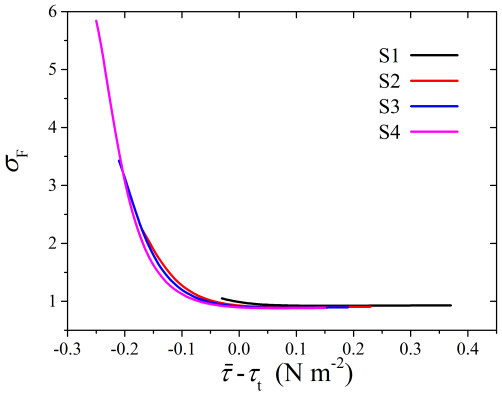

Figure 7. Relationship between σ_F and excess surface shear stress ($\overline{\tau} - \tau_t$).

indicating relatively small influence from the quasi-convective turbulence. But for the conditions with $\overline{\tau} < \tau_t$, σ_F significantly increase with decreasing $\overline{\tau} - \tau_t$, reaching up to 6 at $\overline{\tau} - \tau_t$ = - 0.25 Nm^{-2}, indicating that the influence of convective turbulence is significant (corresponding to the intermittent entrainment defined by Li et al. 2020). We can thus conclude that convective turbulence may significantly enhance dust entrainment by alter how shear stress acts on the surface, especially for the cases of intermittent entrainment in weak mean wind conditions.

3 Conclusions

In this study, we carried out wind-tunnel experiments and studied the influences of turbulence structure on aerodynamic entrainment of sand and dust particles. We considered τ to be a stochastic variable and showed that the probabilistic distribution of τ (i.e. $p(\tau)$), in addition to the mean surface shear stress $\overline{\tau}$, has a significant impact on aeolian fluxes, since the entrainment rate of sand and dust particles depends non-linearly on surface shear stress, τ. Because the fluctuations of τ are closely related to the structure of ABL turbulence, aeolian fluxes in ABLs of different stabilities can be substantially different even if $\overline{\tau}$ is

https://doi.org/10.5194/acp-2022-76
Preprint. Discussion started: 17 March 2022


Atmospheric Chemistry and Physics Discussions

the same. The wind-tunnel experiments provided direct data which show that ABL convective large eddies are of particular importance to the entrainment of sand and dust particle, as they intermittently generate large shear stress on the surface.

Wind-tunnel flows are normally neutrally stratified and do not contain large eddies similar to those in convective ABLs. By examining the power spectra of turbulence for the NP runs, we showed that wind-tunnel turbulence lacks energy containing eddies even compared with ABL flows in neutral conditions, highlighting the deficiency of traditional wind-tunnel experiments on aeolian studies. We showed that the deployment of a piece of fluttering cloth is both simple and effective in generating quasi-convective turbulence. By comparing the power spectra of turbulence for the WP runs and NP runs, we found that the energy density in the large eddy range substantially increased. The energy spectrum of quasi-convective eddies agrees reasonably well with that of turbulence in unstable ABL with z/L = -2. Although the employment of the forced-perturbation technique did not fully reproduce the energy spectra of convective turbulence, this simple technique can be further developed and optimized to obtain the desired turbulent features and overcome a vital limitation to the wind-tunnel experiments.

By comparing the WP runs and NP runs, we found that quasi-convective turbulence increases the mean value (just as in convective ABLs) as well as the variance and skewness of the surface shear stress, all contributing to the entrainment of sand and dust particles. For a given mean shear stress, the entrainment rate for the WP runs is substantially higher than for the NP runs, i.e., convective turbulence is more effective than neutral turbulence in entraining particles into the atmosphere.

The findings of this study obtained through wind-tunnel observations are consistent with the results of Shao et al. (2020). The latter authors showed based on field observations that the PDF of u_* profoundly influences the magnitude of saltation flux, Q. With fixed u_* mean, a larger u_* variance corresponds to a larger Q. Unstable ABL has in general larger u_* variances which generate stronger saltation bombardment and produce the emission of finer dust particles, and saltation in unstable ABLs is generally more fully developed and saltation bombardment has higher intensity. In a more recent study, Yin et al. (2021) demonstrated using large-eddy simulations that also dust deposition is strongly affected by the structure of turbulence. Together with the earlier studies of Shao (2008), Klose and Shao (2012), Klose et al. (2014), Li et al. (2020), Khalfallah et al. (2020), Shao et al. (2020), and Yin et al. (2021), we have shown the critical importance of taking into consideration of turbulence structure in aeolian studies and partly quantified the impact of turbulence on sand and dust entrainment, saltation fluxes, and dust deposition.

Data availability. Data is available from Dr. Zhang (zhang-j@lzu.edu.cn) or Dr. Li (liguang@lzu.edu.cn) on requests.

Author contributions. Yaping Shao and Jie Zhang conceived and designed the wind tunnel experiment; Jie Zhang, Guang Li, and Li Shi carried out the experiment, performed the data analyses, and prepared the first draft; Yaping Shao and Ning Huang organized this study and contributed to its conceptualization, discussions, and finalization of the paper.

https://doi.org/10.5194/acp-2022-76
Preprint. Discussion started: 17 March 2022

Atmospheric Chemistry and Physics Discussions

Competing interests. The authors declare that they have no conflict of interest.

Acknowledgements. This work is supported by the State Key Program of National Natural Science Foundation of China (41931179, 42006187), the Major Science and Technology Project of Gansu Province (21ZD4FA010), the Second Tibetan Plateau Scientific Expedition and Research Program (2019QZKK020611), and the Fundamental Research Funds for the Central Universities (lzujbky-2020-cd06).

https://doi.org/10.5194/acp-2022-76
Preprint. Discussion started: 17 March 2022

Atmospheric Chemistry and Physics Discussions

References

Alfaro, S. C., Gaudichet, A., Gomes, L., and Maillé, M.: Modeling the size distribution of a soil aerosol produced by sandblasting, J. Geophys. Res. Atmos., 102, 11 239–11 249, https://doi.org/10.1029/97jd00403, 1997.

Anderson, R. S. and Haff, P.: Wind modification and bed response during saltation of sand in air, in: Aeolian Grain Transport 1, pp. 21–51, Springer, https://doi.org/10.1007/978-3-7091-6706-9_2, 1991.

Anderson, R. S. and Haff, P. K.: Simulation of Eolian Saltation, Science, 241, 820–823, https://doi.org/10.1126/science.241.4867.820, 1988.

Bagnold, R. A.: The physics of blown sand and desert dunes, Methuen, New York, https://doi.org/10.1007/978-94-009-5682-7, 1941.

Brown, S., Nickling, W., and Gillies, J.: A wind tunnel examination of shear stress partitioning for an assortment of surface roughness distributions, J. Geophys. Res. Earth Surf., 113, https://doi.org/10.1029/2007jf000790, 2008.

Businger, J. A., Wyngaard, J. C., Izumi, Y., and Bradley, E. F.: Flux-profile relationships in the atmospheric surface layer, J. Atmos. Sci, 28, 181–189, https://doi.org/10.1175/1520-0469(1971)028<0181:fprita>2.0.co;2, 1971.

Butterfield, G.: Grain transport rates in steady and unsteady turbulent airflows, in: Aeolian Grain Transport 1, pp. 97–122, Springer, https://doi.org/10.1007/978-3-7091-6706-9_6, 1991.

Butterfield, G. R.: Transitional behaviour of saltation: wind tunnel observations of unsteady winds, J. Arid. Environ., 39, 377–394, https://doi.org/10.1006/jare.1997.0367, 1998.

Comola, F., Kok, J. F., Chamecki, M., and Martin, R. L.: The Intermittency of Wind-Driven Sand Transport, Geophys. Res. Lett., 46, 13 430–13 440, https://doi.org/https://doi.org/10.1029/2019GL085739, 2019.

Doorschot, J. J. and Lehning, M.: Equilibrium saltation: mass fluxes, aerodynamic entrainment, and dependence on grain properties, Boundary Layer Meteorol., 104, 111–130, https://doi.org/10.1023/a:1015516420286, 2002.

Gillette, D. A., Herbert, G., Stockton, P. H., and Owen, P.: Causes of the fetch effect in wind erosion, Earth Surf. Processes Landforms, 21, 641–659, https://doi.org/10.1002/(sici)1096-9837(199607)21:7<641::aid-esp662>3.0.co;2-9, 1996.

Gillette, D. A., Hardebeck, E., and Parker, J.: Large-scale variability of wind erosion mass flux rates at Owens Lake: 2. Role of roughness change, particle limitation, change of threshold friction velocity, and the Owen effect, J. Geophys. Res. Atmos., 102, 25 989–25 998, https://doi.org/10.1029/97jd00960, 1997.

Gillies, J. A., Nickling, W. G., and King, J.: Shear stress partitioning in large patches of roughness in the atmospheric inertial sublayer, Boundary Layer Meteorol., 122, 367–396, https://doi.org/10.1007/s10546-006-9101-5, 2007.

Greeley, R. and Iversen, J. D.: Wind as a geological process: on Earth, Mars, Venus and Titan, 4, CUP Archive, https://doi.org/10.1017/cbo9780511573071, 1987.

Irwin, H. P. A.: A simple omnidirectional sensor for wind-tunnel studies of pedestrian-level winds, J. Wind Eng. Ind. Aerodyn., 7, 219–239, https://doi.org/10.1016/0167-6105(81)90051-9, 1981.

Ishizuka, M., Mikami, M., Leys, J., Yamada, Y., Heidenreich, S., Shao, Y., and McTainsh, G.: Effects of soil moisture and dried raindroplet crust on saltation and dust emission, J. Geophys. Res. Atmos., 113, https://doi.org/10.1029/2008jd009955, 2008.

Ishizuka, M., Mikami, M., Leys, J. F., Shao, Y., Yamada, Y., and Heidenreich, S.: Power law relation between size-resolved vertical dust flux and friction velocity measured in a fallow wheat field, Aeolian Res., 12, 87–99, https://doi.org/10.1016/j.aeolia.2013.11.002, 2014.

Jia, S. and Wang, Z.: Simulation of aerodynamic entrainment with interparticle cohesions based on discrete element method, Earth Surf. Process. Landf., 46, 1410–1418, https://doi.org/https://doi.org/10.1002/esp.5109, 2021.

https://doi.org/10.5194/acp-2022-76
Preprint. Discussion started: 17 March 2022

Atmospheric Chemistry and Physics Discussions

Kaimal, J. C. and Finnigan, J. J.: Atmospheric boundary layer flows: their structure and measurement, Oxford university press, https://doi.org/10.1093/oso/9780195062397.001.0001, 1994.

Kaimal, J. C., Wyngaard, J., Izumi, Y., and Coté, O.: Spectral characteristics of surface-layer turbulence, Quart. J. Roy. Meteor. Soc., 98, 563–589, https://doi.org/10.1002/qj.49709841707, 1972.

Khalfallah, B., Bouet, C., Labiadh, M., Alfaro, S., Bergametti, G., Marticorena, B., Lafon, S., Chevaillier, S., Féron, A., Hease, P., et al.: Influence of atmospheric stability on the size distribution of the vertical dust flux measured in eroding conditions over a flat bare sandy field, Journal of Geophysical Research: Atmospheres, 125, e2019JD031 185, https://doi.org/10.1029/2019JD031185, 2020.

Klose, M. and Shao, Y.: Stochastic parameterization of dust emission and application to convective atmospheric conditions, Atmos. Chem. Phys., 12, 7309–7320, https://doi.org/10.5194/acpd-12-3263-2012, 2012.

Klose, M., Shao, Y., Li, X., Zhang, H., Ishizuka, M., Mikami, M., and Leys, J. F.: Further development of a parameterization for convective turbulent dust emission and evaluation based on field observations, J. Geophys. Res. Atmos., 119, 10 441–10 457, https://doi.org/10.1002/2014jd021688, 2014.

Leys, J. F.: Wind erosion processes and sediments in southeastern Australia, Ph.D. thesis, Griffith University, 1998.

Li, G., Zhang, J., Herrmann, H., Shao, Y., and Huang, N.: Study of aerodynamic grain entrainment in aeolian transport, Geophys. Res. Lett., 47, e2019GL086 574, https://doi.org/10.1029/2019GL086574, 2020.

Liu, D., Ishizuka, M., Mikami, M., and Shao, Y.: Turbulent characteristics of saltation and uncertainty of saltation model parameters, Atmos. Chem. Phys., 18, 7595–7606, https://doi.org/10.5194/acp-18-7595-2018, 2018.

Loosmore, G. A. and Hunt, J. R.: Dust resuspension without saltation, J. Geophys. Res. Atmos., 105, 20 663–20 671, https://doi.org/10.1029/2000jd900271, 2000.

Owen, P. R.: Saltation of uniform grains in air, J. Fluid Mech., 20, 225–242, https://doi.org/10.1017/s0022112064001173, 1964.

Raffaele, L., Bruno, L., Pellerey, F., and Preziosi, L.: Windblown sand saltation: A statistical approach to fluid threshold shear velocity, Aeolian Res., 23, 79–91, https://doi.org/10.1016/j.aeolia.2016.10.002, 2016.

Rasmussen, K. and Mikkelsen, H.: Wind tunnel observations of aeolian transport rates, in: Aeolian Grain Transport 1, pp. 135–144, Springer, https://doi.org/10.1007/978-3-7091-6706-9_8, 1991.

Shao, Y.: Physics and modelling of wind erosion, vol. 37, Springer Science & Business Media, https://doi.org/10.1007/978-1-4020-8895-7, 2008.

Shao, Y., Zhang, J., Ishizuka, M., Mikami, M., Leys, J., and Huang, N.: Dependency of particle size distribution at dust emission on friction velocity and atmospheric boundary-layer stability, Atmos. Chem. Phys., 20, 12 939–12 953, https://doi.org/10.5194/acp-20-12939-2020, 2020.

Stout, J. and Zobeck, T.: Intermittent saltation, Sedimentology, 44, 959–970, https://doi.org/10.1046/j.1365-3091.1997.d01-55.x, 1997.

Walter, B., Gromke, C., Leonard, K., Clifton, A., and Lehning, M.: Spatially resolved skin friction velocity measurements using Irwin sensors: a calibration and accuracy analysis, J. Wind Eng. Ind. Aerodyn., 104, 314–321, https://doi.org/10.1016/j.jweia.2012.02.018, 2012.

Wiernga, J.: Representative roughness parameters for homogeneous terrain, Boundary Layer Meteorol., 63, 323–363, https://doi.org/10.1007/bf00705357, 1993.

Wu, H. and Stathopoulos, T.: Wind-tunnel techniques for assessment of pedestrian-level winds, J. Eng. Mech., 119, 1920–1936, https://doi.org/10.1061/(asce)0733-9399(1993)119:10(1920), 1993.

Xuan, J.: Turbulence factors for threshold velocity and emission rate of atmospheric mineral dust, Atmos. Environ., 38, 1777–1783, https://doi.org/https://doi.org/10.1016/j.atmosenv.2003.12.030, 2004.

https://doi.org/10.5194/acp-2022-76
Preprint. Discussion started: 17 March 2022

315 Yin, X., Jiang, C., Shao, Y., Huang, N., and Zhang, J.: LES study on turbulent dust deposition and its dependence on atmospheric boundary-layer stability, Atmospheric Chemistry and Physics Discussions, [preprint], https://doi.org/10.5194/acp-2021-809, 2021.

Zhang, J., Shao, Y., and Huang, N.: Measurements of dust deposition velocity in a wind-tunnel experiment, Atmos. Chem. Phys., 14, 8869–8882, https://doi.org/10.5194/acpd-14-9439-2014, 2014.